

Vortex arrays in nanoscopic superfluid helium droplets

Francesco Ancilotto,^{1,2} Martí Pi,³ and Manuel Barranco³

¹*Dipartimento di Fisica e Astronomia “Galileo Galilei” and CNISM,
Università di Padova, via Marzolo 8, 35122 Padova, Italy*

²*CNR-IOM Democritos, via Bonomea, 265 - 34136 Trieste, Italy*

³*Departament ECM, Facultat de Física, and IN²UB,
Universitat de Barcelona. Diagonal 645, 08028 Barcelona, Spain*

(Dated: June 24, 2021)

We have studied the appearance of vortex arrays in a rotating ^4He nanodroplet at zero temperature within density functional theory. Our results are compared with those for classical rotating fluid drops used to analyze the shape and vorticity in recent experiments [L.F. Gomez et al., *Science* **345**, 906 (2014)], where vortices have been directly seen in superfluid droplets for the first time. In agreement with the experiments, we have found that the shape of the droplet changes from pseudo-spheroid, oblate-like for a small number of vortices to a peculiar “wheel-like” shape, delimited by nearly flat upper and lower surfaces, when the number of vortices is large. Also in agreement with the experiments, we have found that the droplet remains stable well above the stability limit predicted by classical theories.

PACS numbers: 67.25.D-, 67.25.dk, 67.25.dr

Helium-4 droplets created by expanding a cold helium gas¹ or fragmentation of a cryogenic liquid attain a limiting temperature below 0.4 K,² and constitute the only self-bound superfluid systems. Superfluidity in helium droplets was established through the dissipationless rotation of an OCS molecule inside them, as indicated by the appearance of a clean ro-vibrational spectrum.³ More recently, the indirect evidence of quantum vortices^{4–6} and the frictionless displacement of swift impurities in helium droplets⁷ point towards a superfluid character of helium nanodroplets.

Superfluid ^4He droplets cannot be set into rotation as ordinary droplets or rigid bodies. If a rotating helium droplet in the normal phase above the superfluid transition temperature $T_\lambda = 2.17$ K is cooled down reaching the superfluid phase, it reacts by storing its angular momentum either into quantized vortices or into travelling capillary waves.⁸ Conversely, a critical angular velocity ω_c has to be supplied to the superfluid droplet for the nucleation of vortices with quantized velocity circulation in units of h/M , where h is the Planck constant and M is the mass of a ^4He atom. Single vortices in helium droplets have been addressed theoretically by methods of different complexity, see e.g. Refs. 9–13.

When the angular velocity is increased above ω_c , larger amounts of angular momentum may be stored into the superfluid by increasing the number of nucleated vortices. These vortices arrange themselves into ordered structures (lattices) whose existence in bulk superfluid ^4He was established long ago.^{14,15} We refer the reader to Refs. 16–18 for a general presentation of the subject.

Very recently, superfluid He nanoscopic droplets in fast rotation have been studied by coherent X-ray scattering.¹⁹ The existence of vortex lattices inside the droplets was established by the appearance of Bragg patterns from Xe clusters trapped in the vortex cores in droplets made of $N = 10^8 - 10^{11}$ atoms (corresponding to

radii from 100 to 1000 nm) produced by the fragmentation of liquid helium expanding into vacuum. The shapes of the droplets were consistent with those of axially symmetric oblate pseudo-spheroids with large aspect ratio (AR), defined as the ratio of the long half-axis length b to the short half-axis length a along the rotational axis. While normal liquid drops change their shape as rotation becomes faster^{20–22} to resemble a “peanut” (multi-lobe shape) or a “blood cell”, no evidence of such shape shifting has been seen in the helium nanodroplets.¹⁹ As shown in the following, this is fully confirmed by our calculations.

The presence of dopants was instrumental for detecting the vortex cores, although their number was sensibly smaller than the number of helium atoms ($N_{\text{Xe}} \sim 10^{-3}N_{\text{He}}$) and their presence is not expected to introduce large deformations in the droplet in spite that they locally distort the superfluid around them, see e.g. Refs. 10,23. Possible effects on the distribution of vortex cores inside the droplet might come from the additional rotational energy associated to the Xe mass, especially at the periphery of the droplet. Although such effects seem to have been observed occasionally in the experimental images of Ref. 19, we will not consider them here. In the case of a rotating nanocylinder, these distortions were found to be negligible.²³

Once experimentally established the presence of a vortex lattice in a droplet of aspect ratio b/a , the number N_v of vortices in the lattice could be determined approximately from the vortex areal density (Feynman’s formula²⁴)

$$n_v \equiv N_v/S = 2M\omega/h \quad (1)$$

where ω is the rotational angular velocity and $S = \pi b^2$ is the equatorial cross section of the droplet. Since ω cannot be directly determined in the experiment,¹⁹ the anal-

ysis relies on the classical relationship between the AR – experimentally accessible through the diffraction contour maps – and the angular velocity, whose connection with the parameters a and b is given by the classical theories of rotating liquid drops.^{20,21} In this way the experiments estimated that the number of vortices in a single droplet could be as large as $N_v = 160$. When the vortex density is particularly large the experimental images showed also the occurrence of “wheel-shaped” droplets¹⁹ which have no classical counterpart.

The distinct features of superfluid helium, namely its irrotational flow and the possible appearance of quantized vortices, are of course not included in the classical rotating droplet model.^{20,21} The existence of a large vortex lattice might influence the appearance of the rotating droplet, and the irrotational moment of inertia is known to be very different from that of the rigid body.²⁵ These facts call for theoretically addressing rotating helium droplets with accurate methods which have proven to provide reliable results for superfluid ^4He in confined geometries.

We present here a Density Functional Theory (DFT) study at zero temperature of pure superfluid helium droplets hosting an increasing number of vortices. To our knowledge, this is the first realistic study of multi-vortex configurations in ^4He nanodroplets. A previous attempt to study multi-vortex configurations in superfluid droplets is described in Ref. 26, where a simplified model assuming linear vortices and a rigid spherical droplet was used.

We have recently analyzed a simpler model system, namely a rotating superfluid ^4He nanocylinder hosting arrays of linear vortex lines,²³ that constitutes the starting point of the present study. Within our approach, a self-bound superfluid ^4He droplet is described by a complex effective wave function $\Psi(\mathbf{r}, t)$ related to its atomic density as $\rho(\mathbf{r}, t) = |\Psi(\mathbf{r}, t)|^2$. In the fixed-droplet frame of reference (corotating frame) we seek for stationary solutions $\Psi(\mathbf{r}, t) = e^{-i\mu t/\hbar}\Phi(\mathbf{r})$, where the chemical potential μ and the time-independent effective helium wave function Φ are obtained by solving the time-independent equation

$$[\hat{H} - \omega \hat{L}_z] \Phi(\mathbf{r}) = \mu \Phi(\mathbf{r}), \quad (2)$$

where \hat{H} is the DFT Hamiltonian,²⁷ \hat{L}_z is the angular momentum operator around the z -axis, and ω is the angular velocity of the corotating frame.

To determine $\Phi(\mathbf{r})$ describing a configuration where N_v vortex lines are present we follow the “imprinting” strategy, i.e. we start the imaginary-time evolution of Eq. (2) leading to the minimum energy configuration with a helium wave function²³

$$\Phi_0(\mathbf{r}) = \sqrt{\rho_0(\mathbf{r})} \sum_{j=1}^{N_v} \left[\frac{(x - x_j) + i(y - y_j)}{\sqrt{(x - x_j)^2 + (y - y_j)^2}} \right] \quad (3)$$

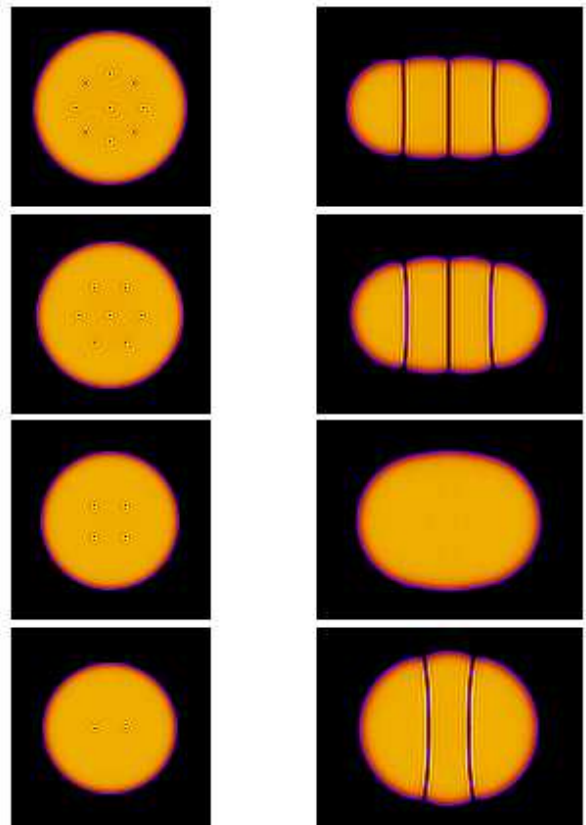


FIG. 1: Helium droplet configurations hosting (from bottom to top) $N_v = 2, 4, 7,$ and 9 vortices. The left column shows the density in the $z = 0$ symmetry plane (top view), while the right column shows side views ($x = 0$ plane).

where $\rho_0(\mathbf{r})$ is the density of the vortex-free droplet and (x_j, y_j) is the initial position of the j -vortex linear core with respect to the z -axis of the droplet. During the functional minimization the vortex positions will change to provide, at convergence, the lowest energy vortex configuration. It is worth stressing that we work in Cartesian coordinates and that no symmetry is imposed to the solutions of Eq. (2). We refer the reader to Ref. 23 and references therein for technical details on how this equation has been solved.

Due to the high computational cost of our calculations, we have limited this study to a helium droplet made of $N_{\text{He}} = 15000$ helium atoms having a radius $R = r_0 N_{\text{He}}^{-1/3}$ with $r_0 = 2.22 \text{ \AA}$, i.e., $R = 54.7 \text{ \AA}$. This droplet is still much smaller than the experimental ones, which in turn limits the number of hosted vortices. However, our findings can be compared with the experimental results on much larger droplets once scaled with a dimensionless characteristic rotational velocity Ω defined as²¹

$$\Omega = \sqrt{\frac{M \rho_0 R^3}{8 \gamma}} \omega, \quad (4)$$

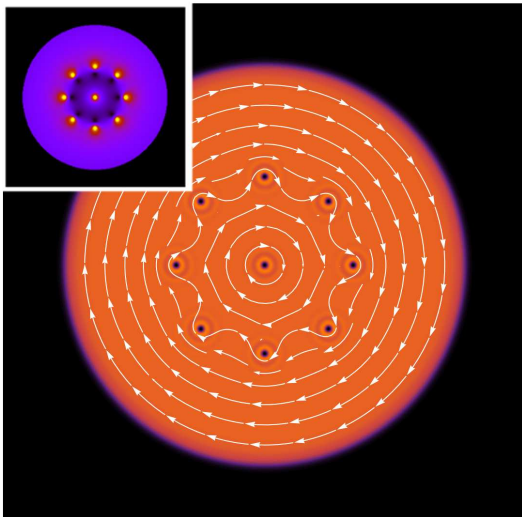


FIG. 2: Circulation lines of the velocity field corresponding to the $N_v = 9$ configuration of Fig. 1. The inset displays in a color scale the regions around the vortex cores where the modulus of the velocity field is higher (bright spots). The dark spots are regions of low vorticity due to the interference between the velocity fields of neighboring vortices.

where $\rho_0 = 0.0218 \text{ \AA}^{-3}$ is the helium atom density and $\gamma = 0.274 \text{ K \AA}^{-2}$ is the surface tension of the liquid. For the $N_{\text{He}} = 15000$ droplet, $\Omega = 1$ corresponds to $\omega = 1.13 \times 10^{10} \text{ s}^{-1}$.

Figure 1 shows configurations hosting $N_v = 2, 4, 7,$ and 9 vortex arrays obtained with $\Omega = 0.43, 0.54, 0.62,$ and 0.69 , respectively. Comparing the top and lateral views, it is apparent that the droplet becomes increasingly deformed, oblate-like, as N_v (and thus Ω) increases. Also apparent is how the droplet surface locally deforms and the vortex lines bend forced by the physical requirement that their open ends hit perpendicularly the surface. The bending is smaller for larger N_v and, at variance with the classical droplet results,^{20–22} the droplet becomes “wheel-like” as indeed observed in the experiments.¹⁹

By increasing the angular velocity the number of vortices that can be stabilized inside the droplet increases. Eventually, a maximum number of vortices can be hosted, above which the rotating droplet will no longer be stable. For the $N_{\text{He}} = 15000$ droplet we have found that the maximum N_v value is 9.

As in rotating buckets,¹⁶ the higher the angular velocity, the more packed the vortex array is around the rotation axis. This leaves a “strip” around the equator of the droplet free of vortices that can be clearly appreciated in the $N_v = 9$ case as shown in Fig. 2, where we display several circulation lines of the superfluid velocity field. The inset shows in a color scale the regions around the vortex cores where the modulus of the velocity field is higher (bright spots). As expected, the calculated circulation of the velocity field of the superfluid along a path surrounding the vortex array equals N_v , and equals unity

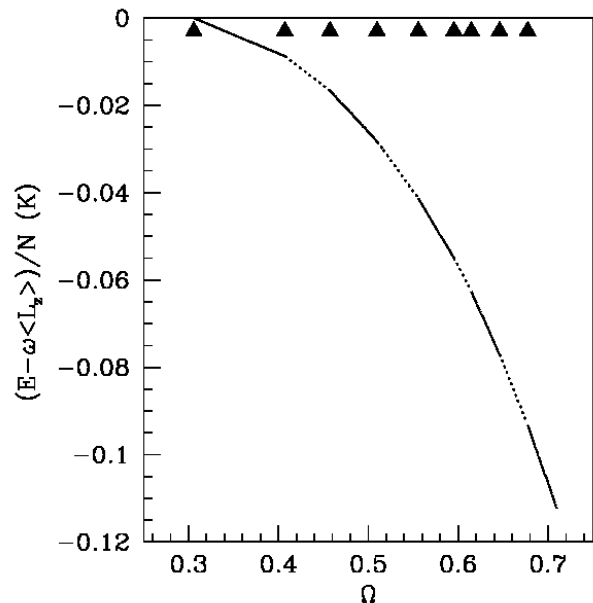


FIG. 3: Stability diagram for a number of vortex lines $N_v = 0, 1, 2, \dots, 9$ as a function of the dimensionless angular velocity Ω . The zero of the energy scale corresponds to the energy of the vortex-free droplet. The vertical axis is the energy per atom in the corotating frame referred to that of the vortex-free droplet. The triangles mark the crossings between different stability lines.

around every single vortex.

Figure 3 shows the calculated stability diagram. As for the rotating bucket,^{23,28,29} the energetically favored structures for $N_v > 5$ are made of a ring of vortices encircling a vortex at the center of the droplet.

It is worth observing that Eq. (1), which strictly applies to an extended vortex triangular (Abrikosov) lattice made of a large number of vortex lines, is also fulfilled in the present case in spite of the limited number of vortices. This occurs in the case of $N_v = 7$, where the equilibrium structure (see Fig. 1), is a “patch” of a triangular lattice whose areal density is $n_v = 2/(\sqrt{3}d^2)$, d being the mean inter-vortex distance. By equating this expression to Eq. (1) –with the value $\Omega = 0.62$ used to obtain the 7-vortex configuration shown in Fig. 1– one gets $d = 28.3 \text{ \AA}$. An average vortex-vortex distance $d = 28.2 \text{ \AA}$ can be estimated from Fig. 1, which compares very well with the result of the classical vortex theory.^{20–22}

Figure 1 shows that, disregarding the vortex array, the shape of the droplet is almost axially symmetric. To determine its AR we have calculated a and b from the moments of the density distribution obtaining³⁰ $b/a = [\langle x^2 \rangle / \langle z^2 \rangle]^{1/2}$, where $\langle x^2 \rangle = \int \rho(\mathbf{r}) x^2 d\mathbf{r}$ and $\langle z^2 \rangle = \int \rho(\mathbf{r}) z^2 d\mathbf{r}$.

The AR dependence on the angular velocity Ω is shown in Fig. 4, together with the curve derived from the classical model for a rotating liquid droplet²⁰, and used in Ref.¹⁹ to interpret their data.

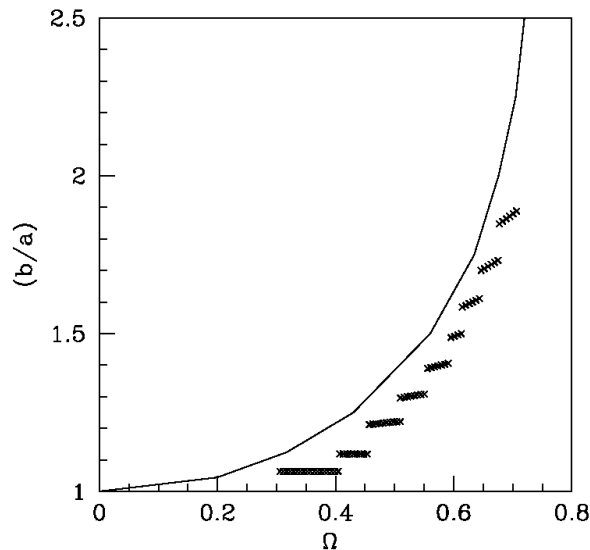


FIG. 4: Aspect ratio b/a as a function of the dimensionless angular velocity Ω . The solid line shows the curve obtained from the classical model for axisymmetric rotating droplets.

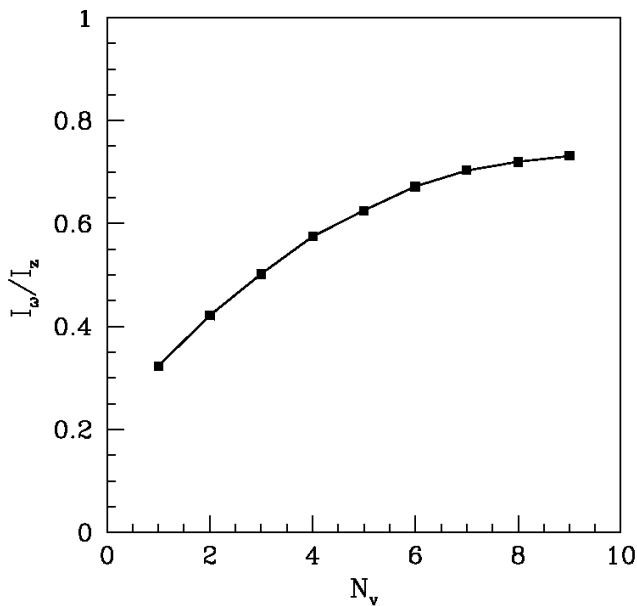


FIG. 5: Calculated ratio I_ω/I_z shown as a function of the number of vortices N_v .

The figure shows that for a given angular velocity, the classical droplet model overestimates the calculated aspect ratio. Most likely, the calculated points in Figs. 4 should get closer to the classical curve for larger droplets

having many vortices, which unfortunately are beyond the current possibilities of the DFT approach. Notice also that in the experiments of Ref. 19 axially symmetric stable droplets were observed with aspect ratios as high as $b/a = 2.3$ corresponding to $\Omega = 0.71$, considerably larger than the shape instability threshold of classical droplets leading to multi-lobe configurations, $\Omega = 0.56$. Our calculations also yield a similar behavior.

It appears from Fig. 4 that as N_v increases the dependence of the AR on Ω within the corresponding stability region (i.e. within each group of crosses shown in Fig.4) becomes increasingly important, i.e. the droplet is more easily deformed. Such increase of the AR proceeds by the flattening of the droplet as the vortex cores are pushed, as the frequency is increased, towards the center of the droplet.

Another interesting difference between classical and superfluid behavior, which is likely related to the deviations from classical theory just discussed, emerges if we look at the ratio between the moment of inertia around the z -axis, I_z calculated from the droplet mass distribution, and that obtained from the response of the superfluid to rotation, $I_\omega = \langle \hat{L}_z \rangle / \omega$. The ratio I_ω/I_z is shown in Fig. 5 as a function of N_v taking for Ω a value in the middle of each stability region. One may notice that the higher the angular velocity the closer the moment of inertia becomes to the rigid-body moment of inertia.

To summarize, within DFT we have shown that the shape of rotating helium droplets hosting a number of vortices evolves from spheroidal at low angular velocities to wheel-like at high angular velocities. On the one hand, multi-lobe configurations present in classical viscid droplets²² are hindered by the appearance of vortex arrays whose regular distribution is hard to accommodate into a peanut-like (or higher lobe number) shapes. On the other hand, the physical requirement that the ends of the vortex lines hit perpendicularly the droplet surface favors their parallel alignment for large vortex arrays, and hence the appearance of wheel-like shapes, as indeed observed in the experiments. Finally, in spite of the apparent differences between normal and superfluid rotating droplets, the classical relationship between the aspect ratio and the angular frequency is fairly fulfilled, the classical relationship underestimating the actual angular frequency by less than 10 % for the relevant, larger vortex arrays. Thus, it can be used with some confidence in the analysis of the experimental results.

We thank Andrey Vilesov for stimulating discussions. This work has been performed under Grants No. FIS2011-28617-C02-01 from DGI, Spain (FEDER) and 2014SGR401 from Generalitat de Catalunya.

¹ J.P. Toennies and A.F. Vilesov, *Angew. Chem. Int. Ed.* **43**, 2622 (2004).

² M. Hartmann, R.E. Miller, J. P. Toennies, and A.F.

Vilesov, *Phys. Rev. Lett.* **75**, 1566 (1995).

³ S. Grebenev, J.P. Toennies, and A. Vilesov, *Science* **279**, 2083 (1998).

- ⁴ L.F. Gomez, E. Loginov, and A. Vilesov, Phys. Rev. Lett. **108**, 155302 (2012).
- ⁵ E. Latimer, D. Spence, C. Feng, A. Boatwright, A.M. Ellis, and S. Yang, Nano Lett. **14**, 2902 (2014).
- ⁶ Ph. Thaler, A. Volk, F. Lackner, J. Steurer, D. Knez, W. Grogger, F. Hofer, and W.E. Ernst, Phys. Rev. B **90**, 155442 (2014).
- ⁷ N.B. Brauer, S. Smolarek, E. Loginov, D. Mateo, A. Hernando, M. Pi, M. Barranco, W.J. Buma, and M. Drabbels, Phys. Rev. Lett. **111**, 153002 (2013).
- ⁸ A. Leal, D. Mateo, A. Hernando, M. Pi, and M. Barranco, Phys. Chem. Chem. Phys. **16**, 23206 (2014).
- ⁹ G.H. Bauer, R.J. Donnelly, and W.F. Vinen, J. Low Temp. Phys. **98**, 47 (1995).
- ¹⁰ F. Dalfovo, R. Mayol, M. Pi, and M. Barranco, Phys. Rev. Lett. **85**, 1028 (2000).
- ¹¹ K.K. Lehmann and R. Schmied, Phys. Rev. B **68**, 224520 (2003).
- ¹² F. Ancilotto, M. Barranco, and M. Pi, Phys. Rev. Lett. **91**, 105302 (2003).
- ¹³ E. Sola, J. Casulleras, and J. Boronat, Phys. Rev. B **76**, 052507 (2007).
- ¹⁴ W.F. Vinen, Proc. Roy. Soc. A **260**, 218 (1961).
- ¹⁵ G.A. Williams and R.E. Packard, Phys. Rev. Lett. **33**, 280 (1974).
- ¹⁶ R.J. Donnelly, *Quantized vortices in helium II*, Cambridge Studies in Low Temperature Physics (Cambridge University Press, Cambridge, U.K. 1991), Vol. 3.
- ¹⁷ L. Pitaevskii and S. Stringari, *Bose-Einstein Condensation*, International Series of Monographs on Physics **116** (Clarendon Press, Oxford 2003).
- ¹⁸ A.L. Fetter, Rev. Mod. Phys. **81**, 647 (2009).
- ¹⁹ L.F. Gomez et al, Science **345**, 906 (2014).
- ²⁰ S. Chandrasekhar, Proc. R. Soc. Phys. Lond. A **286**, 1 (1965).
- ²¹ R.A. Brown and L.E. Scriven, Proc. R. Soc. Phys. Lond. A **371**, 331 (1980).
- ²² R.J.A. Hill and L. Eaves, Phys. Rev. Lett. **101**, 234501 (2008).
- ²³ F. Ancilotto, M. Pi, and M. Barranco, Phys. Rev. B **90**, 174512 (2014).
- ²⁴ R.P. Feynman, Progress in Low Temperature Physics, C.J. Gorter, Editor (North-Holland Publishing Company, Amsterdam 1955), vol. 1, p. 1.
- ²⁵ A. Bohr and B.R. Mottelson, *Nuclear Structure* (W.A. Benjamin Inc. Reading, Massachusetts, U.S.A. 1975), Vol. II App. 6A.
- ²⁶ S.T. Nam, G.H. Bauer, and R.J. Donnelly, J. Korean Phys. Soc. **29**, 755 (1996).
- ²⁷ F. Ancilotto, M. Barranco, F. Caupin, R. Mayol, and M. Pi, Phys. Rev. B **72**, 214522 (2005).
- ²⁸ G.B. Hess, Phys. Rev. **161**, 189 (1967).
- ²⁹ L.J. Campbell and R.M. Ziff, Phys. Rev. B **20**, 1886 (1979).
- ³⁰ We have verified that this gives the same AR as computed by direct inspection of the equidensity contour-line plots obtained from our calculations.